JOURNAL OF MECHANICAL ENGINEERING AND SCIENCES
ISSN: 2289-4659 e-ISSN: 2231-8380
VOLUME 19, ISSUE 1, 2025, 10508 - 10520
DOI: https://doi.org/10.15282/jmes.19.1.2025.6.0823

RESEARCH ARTICLE

Numerical investigation on the scale-down approach of Harwell furnace

A. B. Makwana, Rupesh. D. Shah*

Department of Mechanical Engineering, Sardar Vallabhbhai National Institute of Technology, Surat 395007, Gujarat, India
Phone: +910261-2201785, Fax.: 0261-2227334

ABSTRACT - Conducting experimental studies with prototypes is both costly and time-intensive. Scaled-down models can be used for initial experiments. However, scaling requires high precision and clarity. The present study aims to evaluate and compare various scaling approaches for predicting prototype results and to relate the temperature distribution of the scaled model to that of the prototype. Steady-state simulations were carried out using the k–ε turbulence closure model and the probability density function approach. Temperature profiles and stream traces from different scaling methods were compared to identify the optimum scale-down method. Simulation results showed a change in the position of the combustion core; the radial temperature profiles for scale-down models with 50% heat input showed a significant deviation of about 85% at an axial position of 0.1 m, while for the rest of the axial positions, the difference was less than 7%. The results reveal that geometrically larger models align more closely with experimental data, particularly when using the Constant Residence Time (CRT) method, compared to smaller-scale models. To account for the dependency of temperature on energy input and energy release at specific locations within the combustor, a non-dimensional temperature variable, θ was introduced. A comparison of results indicates that the CRT method effectively scales down the combustor, showing strong agreement with experimental data from the literature. The variation in θ for scaled-down models aligns closely with prototype and experimental results, with maximum deviations of 17%. This suggests that θ is a novel and effective variable for establishing reliable connections between scaled-down models and prototypes.

ARTICLE HISTORY
Received : 11th July 2024
Revised : 31st Dec. 2024
Accepted : 27th Feb. 2025
Published : 30th Mar. 2025

KEYWORDS
Prototype
Harwell combustor
Scale down methods
Non dimensional temperature
Constant resident time

1. INTRODUCTION

The scale-down model offers an economical way to conduct experiments compared to a full-scale combustor geometry. Research on scaling up combustors is more general, while studies on scaling down models are rare [1]. The important aspects of scaling are the similarity of nondimensional numbers and the scaling methods. It is essential for designing experiments and simulations that scaled-down or scaled-up models accurately reflect the prototype performance. Scaling up from laboratory to industrial scale involves complexities that cannot be fully captured by a single scaling method having different capacities and conditions. Earlier investigators used different combustors [2-6]. However, the Harwell furnace is widely accepted [7-10] for its simplicity for fundamental studies. The earlier investigators have presented scaling of the combustor using Constant Velocity (CV) and Constant Residence Time, Constant Volume to Jet Momentum Ratio (CM), and Constant Volume to Jet Kinetic Energy Ratio (CK). The investigation by Suksam and Charoensuk [4] examined CV and CRT criteria for pulverized coal, gaseous fuel, and spray oil. They observed that the CV approach increased NOx emissions due to higher retention times. The CRT and CM criteria indicate that increasing air and fuel supply results in intensified pressure within combustors [4, 5, 11, 12]. Scale-up studies comparing CM, CRT, CK and CV criteria are reported in the literature. It was suggested that the burner diameter scaled using the CV method is valid for higher thermal input, while the swirler should be scaled using the CRT method [13].

A large number of scale-up studies are devoted to combustors [2]. Earlier studies have been carried out on a large span of heat input, for example, from 30 kW to 12 MW [4], 2.5 and 50 MW [14]. The scaling is performed in the range of 35 kW to 150 kW [15] and 30 kW to 12 MW [16], demonstrating a significant scale-up of a combustor [17]. More modest scale-up studies range from 3 to 150 kW and 5 MW/m3 [12], 4.75 to 700 kW [3] and 0.58 MW to 5.8 MW [4] are also available. Scaled-up studies are carried out on a larger scale from a base combustor of 3.3 kW to 26 kW [18], 10 kW to 500 kW [5] and 7 kW to 14 MW [19] are reported in the literature. Forming a recirculation zone downstream near the inlet is a crucial factor in the design and operation of the combustor [12,18]. The recirculation zone plays a significant role in mixing, flame stabilization, and combustion. The scaling-up combustor geometry significantly changes the location and rate of recirculation. A scaling-up study by Richter et al. [20] presented a laboratory-scale to semi-industrial-scale study focusing on the inner recirculation zone (IRZ). Through-flow similarity, considering dimensionless surface variable (dimensional less area, the ratio of IRZ surface area to quarl surface area) and velocity variable (ratio minimum velocity in IRZ to mixture velocity), IRZ and reaction are approximately kept in the same area in prototype (original combustor) and scale model. In an earlier study, the dimension is scaled using CV, showing the recirculation rates drop from 280% to 190% while using CRT, the recirculation rates drop from 280% to 220%; the increase in secondary flow

*CORRESPONDING AUTHOR | Rupesh D. Shah | ✉ rds@med.svnit.ac.in
© 2025 The Author(s). Published by Universiti Malaysia Pahang Al-Sultan Abdullah Publishing. This is an open access article under the CC BY-NC 4.0 license

enhanced by 153% to 230% [18]. It was concluded that the new nondimensional number does not provide a significant benefit compared to established correlations. The CV and CRT methods have good potential and merits [15], [19], while CRT would be recommended in the context of pulverized fuel burners [19]. A scale-up study for biomass furnaces is presented using characteristic numbers obtained using dimensional analysis. However, the results obtained from the CFD simulations are expected to conform to the scale-up model [15].

The CV method has primarily attracted researchers to investigate the effect of scaleup on emission, particularly on NO_X. The pulverized fuel jets (found in rotary kilns) are scaled using the CV model. The velocity, temperature profiles, and combustion settings are correctly scaled. However, the CV model is unable to predict NO_X formation from pilot-scale facilities to commercial scale [19]. In the study of Suksam and Charoensuk [5], the NO_X emission using CV is higher than CRT due to higher resident time, while CRT yields similar results to the original prototype. CM and CK are advocated in literature for scale-up, particularly for high input [2]. Turning to scale-down studies, Xie et al. [1] presented a numerical and experimental study with geometric scaled-down models of rectangular combustors from 1/2 to 1/10 using Damköhler numbers, D_{a_1} and Reynolds number, R_e similarities. It is reported that R_e law is a good choice for cold flow analysis, while for reactive flow, R_e law gives a significant difference in the flow field due to changes in velocity [21,22]. Reported works on the ability of nondimensional numbers to predict flow physics in prototypes and models conclude that complete modeling is unfeasible due to the involvement of more than one nondimensional number [18]. Previously reported work on scaling is noteworthy, but the full understanding of scaling principles, especially in combustion systems, remains unclear and needs further investigation. Combining methods or a new approach might help to scale across a wide range of geometrical sizes accurately. No explicit guidelines are available for the suitability of a particular scaling method for a combustor. The philosophy that bridges between results obtained from the model and prototype is not clear. The present work is aimed at filling this gap. The aim is to conduct a numerical investigation to identify, evaluate, and compare various scale-down approaches for predicting results for the prototype and propose a technique to relate the model results with that of the prototype.

2. MATERIAL AND METHODS

In the present study, the cylindrical prototype of the Harwell furnace, as shown in Figure 1, which has a 300 mm diameter, is considered for numerical analysis. Methane is used as fuel, and the air is used as an oxidizer. The total length of the furnace is 900 mm. Fuel is injected into the furnace through a 12 mm diameter central core located on the extreme left face of the furnace. The air required for combustion is introduced through the annulus area located concentrically with the fuel inlet area. The inner and outer diameters of the air annulus area are 16.5 mm and 27.5 mm, respectively. The reactive mixture exits the furnace outlet on the extreme right side. The outlet section has a diameter of 88 mm. Figure 1 shows the detailed geometric configuration of the Harwell furnace, including features for the air and fuel inlets, as well as the overall dimensions. Various scaling methods are used to scale down the above prototype of the Harwell furnace. These scaling methods are described in the following.

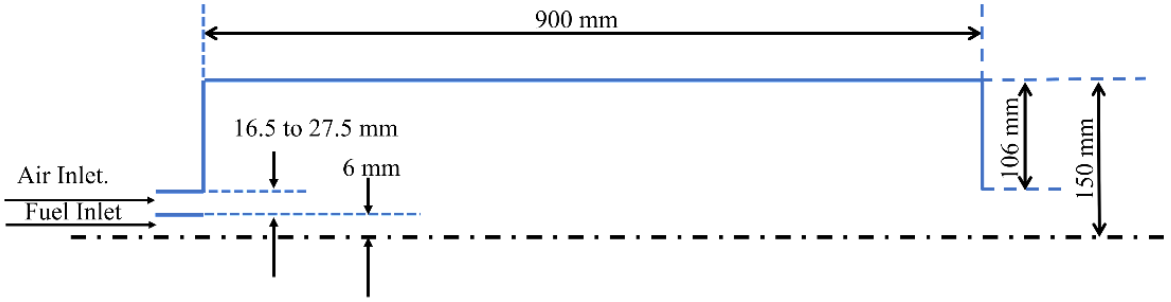

Figure 1. Schematic diagram of Harwell furnace [23]

2.1 Cole Method

In the Cole method, the jet mixing rate and jet natural frequency are maintained constant between the fluid jets of the prototype and that of the model [3]. In this method, the first scaling factor, *S* is fixed. *S* is the ratio of the model geometry's central fluid jet volumetric flow rate, Q_2 to the prototype geometry, Q_1. Using this scaling factor, all the geometrical and velocities are calculated. The modeled jet velocity, V_2 and geometrical dimension, D_2 are derived using the following equations.

$$\frac{V_2}{V_1} = (S)^{\frac{1}{2}} \tag{1}$$

$$\frac{D_2}{D_1} = (S)^{\frac{1}{4}} \tag{2}$$

Despite geometric size and energy input differences, these scaling laws ensure that the fluid flow dynamics and combustion characteristics are similar for the model and their prototype.

2.2 Constant Volume-to-Jet Momentum Ratio

This method keeps the combustor volume to incoming jet momentum and recirculation ratio constant between the model and prototype. The model's velocity and geometrical scaling are derived using the following equations:

$$\frac{D_2}{D_1} = (S)^{\frac{2}{5}} \tag{1}$$

$$\frac{V_2}{V_1} = (S)^{\frac{1}{5}} \tag{2}$$

For the CM scaling method, scaling ensures that the momentum is consistent between the model and the prototype [18], which is crucial for maintaining similarity in fluid flow and combustion characteristics.

2.3 Constant Volume-to-Jet Kinetic Energy Ratio

This method keeps the combustor volume to incoming jet kinetic energy ratio constant between the model and prototype. The recirculation ratio, R_c, which satisfies CV and CRT criteria between injector diameter, D and combustor length, L is maintained constant. For a non-reacting turbulent jet, R_c is given as:

$$R_c \propto \frac{L}{D} \tag{3}$$

The velocity and the geometrical scaling between the model and the prototype are given as:

$$\frac{D_2}{D_1} = (S)^{\frac{3}{7}} \tag{4}$$

$$\frac{V_2}{V_1} = (S)^{\frac{1}{7}} \tag{5}$$

For the CK scaling method, scaling ensures that the momentum and recirculation ratio is consistent between the model and the prototype. This is crucial for maintaining similarity in fluid flow and combustion characteristics [18].

2.4 Constant Resident Time

In constant resident time [24], the time scale of mixing, τ_{mix} is proportional to the ratio characteristics dimension to velocity given as:

$$\tau_{mix} = constant = \frac{D}{V} \tag{6}$$

For the CRT scaling method, the focus is on maintaining the mixing time of the combustible mixture within the combustor. The CRT method ensures that the time available for the fuel and oxidizer to mix and react is similar in both the model and the prototype, preserving the kinetics of the combustion process.

The scaling relation for combustor dimension and velocity are given as:

$$\frac{D_2}{D_1} = (S)^{\frac{1}{3}} \tag{7}$$

$$\frac{V_2}{V_1} = (S)^{\frac{1}{3}} \tag{8}$$

The model developed using CRT may result in larger velocities and significant pressure drops compared to the prototype [12].

2.5 Constant Velocity Method

The constant velocity method [8,9,12] maintains the velocity ratio between the model and the prototype. The scaling relationships are given as:

$$\frac{D_2}{D_1} = (S)^{\frac{1}{2}} \tag{9}$$

$$\frac{V_2}{V_1} = constant \tag{10}$$

The CV method reduces the energy rate [5]. The CV method analysis results in a significant pressure drop and predicts higher CO and NOx emissions than the prototype [6]. The present study examines how scaling down the combustor geometry impacts temperature distribution. Initially, simulations are conducted by reducing the energy input of the full-scale prototype from 55.73 kW to 50% (27.86 kW). Simulations are carried out using scaled velocity and geometrical dimensions using Eqs. (1) to (12). The inlet conditions derived for every modeling approach are listed in Table 1. These details are used for numerical simulation considering different scale-down approaches. In Table 1, Q is the heat supplied,

Uf is the velocity of fuel, Rf, is the radius of the fuel inlet, Uair axial and Ut is the axial and tangential velocity of air, Rair inner, Rair outer, R outlet, and Rmax are the inner, outer radius of air, radius of outlet and maximum radius of combustor, L is the length of combustor, Q''' is the energy input per unit volume. A 2D axisymmetric flow domain is generated, and governing equations are solved using a commercially available CFD tool of Fluent.

Table 1. Model dimensions and flow variables for 50% energy input

Velocity Scaling Factor		constant	0.7937	0.8706	0.9057	0.7071
Geometric Scaling Factor	Full scale	0.7071	0.7937	0.7579	0.7430	0.8409
		CV	CRT	CM	CK	Cole
Q (kW)	55.73	27.86	27.86	27.86	27.86	27.86
U_f (m/s)	15.00	15.00	11.91	13.06	13.59	10.61
R_f (mm)	6.00	4.24	4.76	4.55	4.46	5.05
U_{air} axial (m/s)	12.80	12.80	10.16	11.14	11.59	9.05
U_t (m/s)	6.27	6.27	4.98	5.46	5.68	4.43
$R_{air\ inner}$ (mm)	16.50	11.67	13.10	12.50	12.26	13.87
$R_{air\ outer}$ (mm)	27.50	19.45	21.83	20.84	20.43	23.12
R_{outlet} (mm)	44.00	31.11	34.92	33.35	32.69	37.00
R_{max} (mm)	150.00	106.07	119.06	113.68	111.45	126.13
L (mm)	900.00	636.40	714.33	682.07	668.70	756.81
Q''' (MW/m^3)	0.88	1.24	0.88	1.01	1.07	0.74

2.6 Numerical Model and Grid Independence Study

In the present numerical investigation, simulations are carried out using an axisymmetric, steady-state framework with a pressure-based solver. The general implementation of the governing equation used for a solution using ANSYS® Fluent, Release 2024 R1, is summarized here.

The equation for conversion of mass is given by:

$$\frac{\partial(\bar{\rho}\widetilde{u_r})}{\partial r} + \frac{\partial(\bar{\rho}\widetilde{u_z})}{\partial z} + \frac{(\bar{\rho}\widetilde{u_r})}{r} = 0 \tag{11}$$

$\bar{\rho}$ represents the time-dependent change in mean density $\partial(\bar{\rho}\widetilde{u_z})/\partial r$ and $\partial(\bar{\rho}\widetilde{u_z})/\partial r$ radial and axial convection term, $(\bar{\rho}\widetilde{u_z})/r$ geometric divergence term arises due to the cylindrical geometry of the combustion chamber, $\dot{s}_m$ is due to a change in mass due to an air-fuel chemical reaction

The momentum equation is given by:

$$\bar{\rho}\tilde{u}.\nabla\tilde{u} = -\nabla\bar{p} + \nabla.\bar{\tau} + \bar{\rho}\sum_{k=1}^{N} + \bar{\rho}\sum_{k=1}^{N} Y_k\widetilde{f_k} + \nabla.|\bar{\rho}(\tilde{u}\tilde{u} - \widetilde{u}\widetilde{u})| \tag{12}$$

where, $\bar{\rho}\tilde{u}.\nabla\tilde{u}$ or is the convective term, $-\nabla\bar{p}$ is the pressure gradient term, $\nabla.\bar{\tau}$ is the viscous stress terms and $\bar{\rho}(\tilde{u}\tilde{u} - \widetilde{u}\widetilde{u})$ is the scaler flux.

The governing for turbulence kinetic energy, *k* is given as:

$$\frac{1}{r}\frac{\partial(r\bar{\rho}\,\widetilde{u_r}k)}{\partial r} + \frac{\partial(\bar{\rho}\,\widetilde{u_z}k)}{\partial z} = \frac{1}{r}\frac{\partial}{\partial r}\left(r\bar{\rho}\,D_{eff}\frac{\partial k}{\partial r}\right) + \frac{\partial}{\partial z}\left(\bar{\rho}\,D_{eff}\frac{\partial k}{\partial z}\right) + G_k + G_b - \bar{\rho}\varepsilon + S_k \tag{13}$$

Effective diffusivity, D_{eff}) is used for modeling scalar mixing, species diffusion, and thermal transport. The μ is the molecular diffusivity, μ_t is the turbulence viscosity, Sc_t is the turbulence Schmidt number. G_k and G_b are the generated turbulence kinetic energy due to velocity gradient and buoyancy and S_k is the source term.

$$D_{eff} = \mu + \frac{\mu_t}{Sc_t} \tag{14}$$

$$\mu_t = \bar{\rho}C_\mu\frac{k^2}{\varepsilon} \tag{15}$$

The governing for dissipation of turbulence kinetic energy, ε is given as:

$$\frac{1}{r}\frac{\partial(r\bar{\rho}\,\widetilde{u_r}\varepsilon)}{\partial r} + \frac{\partial(\bar{\rho}\,\widetilde{u_z}\varepsilon)}{\partial z} = \frac{1}{r}\frac{\partial}{\partial r}\left(r\bar{\rho}\,D_{eff}\frac{\partial\varepsilon}{\partial r}\right) + \frac{\partial}{\partial z}\left(\bar{\rho}\,D_{eff}\frac{\partial\varepsilon}{\partial z}\right) + C_{1\varepsilon}\frac{\varepsilon}{k}(G_k + G_bC_{3\varepsilon}) - C_{2\varepsilon}\bar{\rho}\,\frac{\varepsilon^2}{k} + S_\varepsilon \tag{16}$$

where, $C_{1\varepsilon}$=1.44, $C_{2\varepsilon}$=1.92, C_μ=0.09, σ_k=1.0, and σ_ε=1.3. The S_k is the source term.

The non-premix combustion model is used with the assumption of no heat loss to the surroundings (adiabatic). The individual species equation is not solved, but the transport equation for the mixture faction is solved, and it is given by:

The mixture fraction, f is calculated as:

$$f = \frac{z_i - z_{i,ox}}{z_{i,fuel} - z_{i,ox}} \tag{17}$$

where, z_i is the element mass fraction for an element *i*, the oxidizer mass fraction is $z_{i,ox}$ and $z_{i,fuel}$. The transport equation for mixture fraction with equal diffusivity of species:

$$\frac{\partial \bar{\rho}\tilde{f}}{\partial t} + \left(\nabla . \bar{\rho}\tilde{u}\tilde{f}\right) = \nabla . \left\{\left[\frac{k}{c_p} + \frac{\mu_t}{\sigma_t}\nabla\tilde{f}\right]\right\} + s_{user\ define} \tag{18}$$

where, k, c_p, σ_t and μ_t are the laminar thermal conductive of fuel-air mixture, specific heat, Prandtl number, and turbulent viscosity, respectively. $s_{user\ define}$ is the source term.

The conversion of mixture fraction transport of mixture fraction variance, $\overline{f'^2}$ equation is given by.

$$\left(\nabla . \bar{\rho}\tilde{u}\overline{f'^2}\right) = \nabla . \left\{\left[\frac{k}{c_p} + \frac{\mu_t}{\sigma_t}\right]\nabla\overline{f'^2}\right\} + c_g\mu_t . \left[\nabla\bar{f}\right]^2 - c_d\rho\frac{\epsilon}{k}\overline{f'^2} \tag{19}$$

where, $f' = f - \bar{f}$. The default values for the constants σ_t, c_g , c_d are 0.85, 2.86, and 2.0 respectively.

The PDF model is calculated using the following equation in the present simulation.

$$p(f) = \frac{f^{\alpha-1}(1-f)^{\beta-1}}{\int f^{\alpha-1}(1-f)^{\beta-1}df} \tag{20}$$

where, $p(f)$ is the shape of the PDF function, and α and β are shape parameters. The species fraction and temperature are obtained using a predefined table with *f*.

The first-order spherical harmonic (P1) approximation of the radiative transfer equation is used in the present simulation. The basic Radiative Transfer Equation (RTD) for a participating medium is given by:

$$\frac{dI}{dL} = -\kappa I + \kappa G \tag{21}$$

where I is the intensity of radiation, L is the path length, G is the intensity of black body radiation ($\sigma T^4/\pi$), and κ is absorption coefficient, which is expressed as:

$$\kappa = \sum_{i=1}^{N} a_{\epsilon,i}\,\kappa_i \tag{22}$$

where N is the number of grey gas, $a_{\epsilon,i}$ is the weighting factor for i^{th} grey gas, κ_i is the absorption coefficient of the i^{th} grey gas.

The total emissivity, ϵ of the gas over a path length, L is given by:

$$\epsilon = \sum_{i=1}^{N} a_{\epsilon,i}\,(1 - e^{\kappa_i pL}) \tag{23}$$

where absorption coefficient $\alpha_{\epsilon,i}$ is estimated from the following equation:

$$\alpha_{\epsilon,i} = -\frac{(1-\epsilon)}{L} \tag{25}$$

The beam length or optical, L is calculated as,

$$L = 3.6\,\frac{V}{A} \tag{26}$$

where V is the fluid volume, and A is the surface area of the flow domain

The inlet velocity of air and fuel is supplied as the velocity-inlet, and outlet pressure is applied at the exit of the combustor. The turbulence in the fuel-air mixture is modeled using the *k*- ε model with enhanced wall treatment [25]. A no-slip condition is applied at the wall of the flow domain. The inlet velocities utilised in the present work are taken from the work of Hosseini et al. [26]. Semi-Implicit Method for Pressure-Linked Equations (SIMPLE) algorithm is employed for pressure-velocity coupling. The diffusion term is handled using a first-order upwind scheme. Radiative heat transfer within the furnace is modeled using the P1 radiation model. The boundary conditions used for the simulation of the full-scale model are specified in Table 2. At the air inlet, both the axial and tangential velocity components are specified. At the fuel inlet, the axial fuel velocity is assigned. The combustor outlet is designated as a pressure outlet with a specified

zero (gauge) pressure condition. The mesh for the simulation is developed using a facility available in ANSYS® Fluent, Release 2024 R1. A grid independence study is conducted to remove the dependency of numerical results on grid size. In the present study, temperature is chosen as a grid independence variable. Its variation along the furnace axis is obtained and plotted for three different grid sizes: 159402, 216,000, and 314,400 elements. The temperature variation profile for 2,16,000 elements deviates largely by around 9% (for Z=z/L > 0.1) compared to the 159402 elements case. The temperature variation results obtained using 3,14,400 elements are comparable to 216,000 elements. Maximum deviations are below 3% for axial position Z > 0.1. Thus, a mesh with 216000 nodes is selected as a grid-independent mesh.

Table 2. Boundary conditions with full-scale furnace

Surface	Axial Velocity (m/s)	Tangential Velocity (m/s)	k (m^2/s^2)	ε (m^2/s^3)
Air inlet	12.8	6.2695	0.790	255.67
Fuel inlet	15.0	-	0.540	79.38
Outlet	-	-	0.004	0.14

3. RESULTS AND DISCUSSION

3.1 Validation

Axial and radial temperature profiles obtained from the present simulation using full-scale geometry (prototype) in Figure 2 are compared with experimental results reported by Wilkes et al. [23]. The same is presented in Figure 2(a), which represents non-dimensional axial ($Z = z/L$, where L is the scaled combustor length) temperature variation. The captured axial temperature profile agrees well with the reported experimental results. Figure 2(b) to 2(e) compares radial ($R = r/R_{max}$, where R_{max} is the maximum radius of the combustor) temperature profiles at various non-dimensional axial stations located at Z = 0.044, 0.11, 0.22, and 0.44, respectively. At Z = 0.044 and Z = 0.11, some discrepancies in nature and deviations in temperature values are observed. Locations Z = 0.044 and Z = 0.11 are very close to air and fuel jet entry and mixing and radial expansion of these jets.

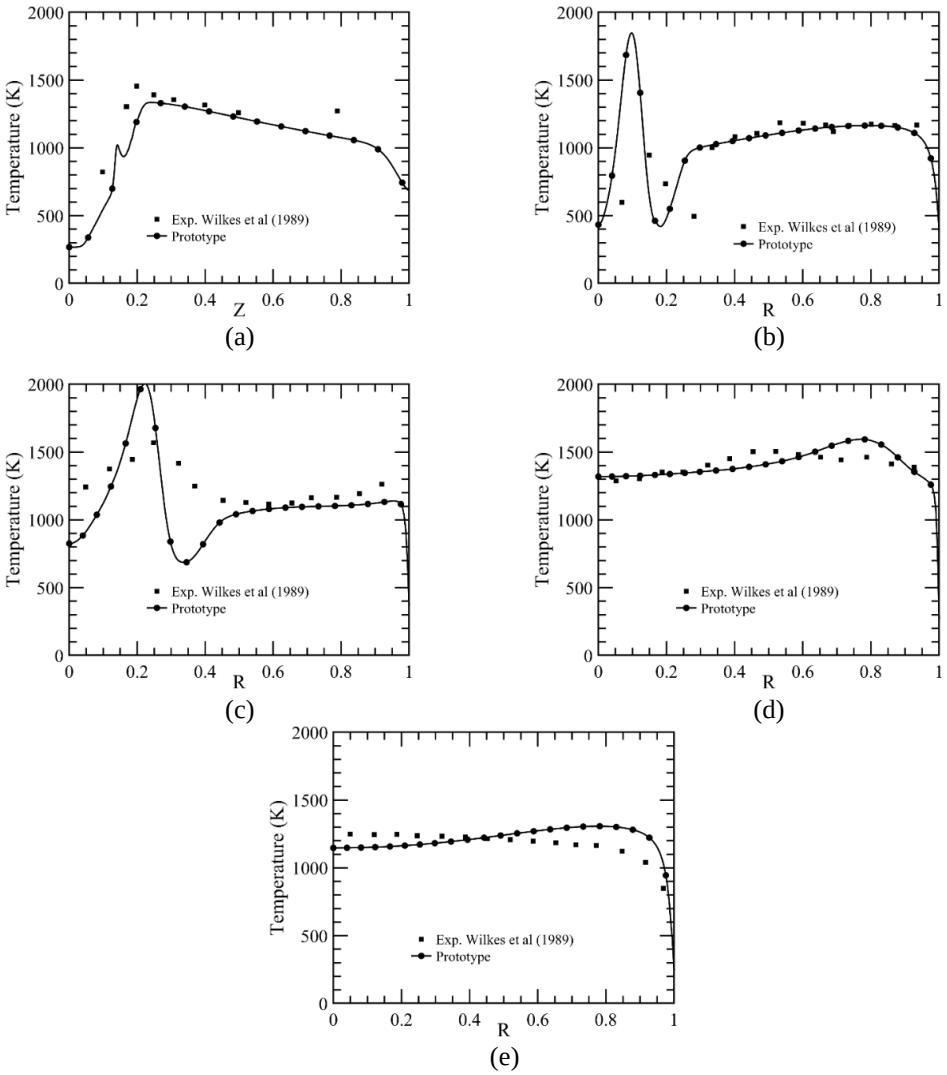

Figure 2. Validation of present simulations: (a) axial variation, (b) Z = 0.044, (c) Z = 0.11, (d) Z = 0.22 and (e) Z = 0.44

Thus, flow physics and chemistry are relatively complex in these regions, which may be the reason for deviation. At stations Z = 0.22 and Z = 0.44, radial temperature profiles agree with the experimental one reported by Wilkes et al. [23]. The comparative assessment of temperature profiles presented in Figure 2 indicates that the results of the present simulations closely align with the experimental investigation by Wilkes et al. [23]. The temperature profiles at some locations deviated from previously reported results by a maximum of 20%. Thus, the computational philosophy used can resolve the involved reactive flow physics.

3.2 Comparison of Temperature Profile for Scaling Methods

Laboratory scaled model dimensions are derived using various approaches discussed above in the section on scaling methods. All these approaches keep the energy input at 50% of the full-scale model. The dimensions of the scaled-down models and associated flow and energy parameters are tabulated in Table 1. These values are used to develop the flow domain and assign boundary values at respective inlet and outlet boundary surfaces. A steady-state simulation is developed for each scaled-down model, and the results are compared with numerical results obtained from the prototype. Figure 3 presents nondimensional axial, Z and radial, R temperature variations. Figure 3(a) illustrates the axial temperature variation for different scale-down modeling approaches at R = 0.2. The temperature increases as the flow progresses toward the exit of the combustor. The minimum difference between the prototype and the models is less than 28% (for CV and CRT), while the difference between CRT and other methods is as small as 3%. These deviations are likely due to differences in geometric dimensions, equivalence ratios, and combustion efficiencies. The CRT temperature profile shows the closest agreement with the prototype. At station Z = 0.044, temperature profiles for all scaling methods nearly overlap and closely match the experimental results. At Z = 0.11 and R = 0.3 (Figure 3(c)), a significant temperature difference is observed between the models and the prototype, with deviations reaching nearly 85% for CM and CRT and at least 38% for CV and CK.

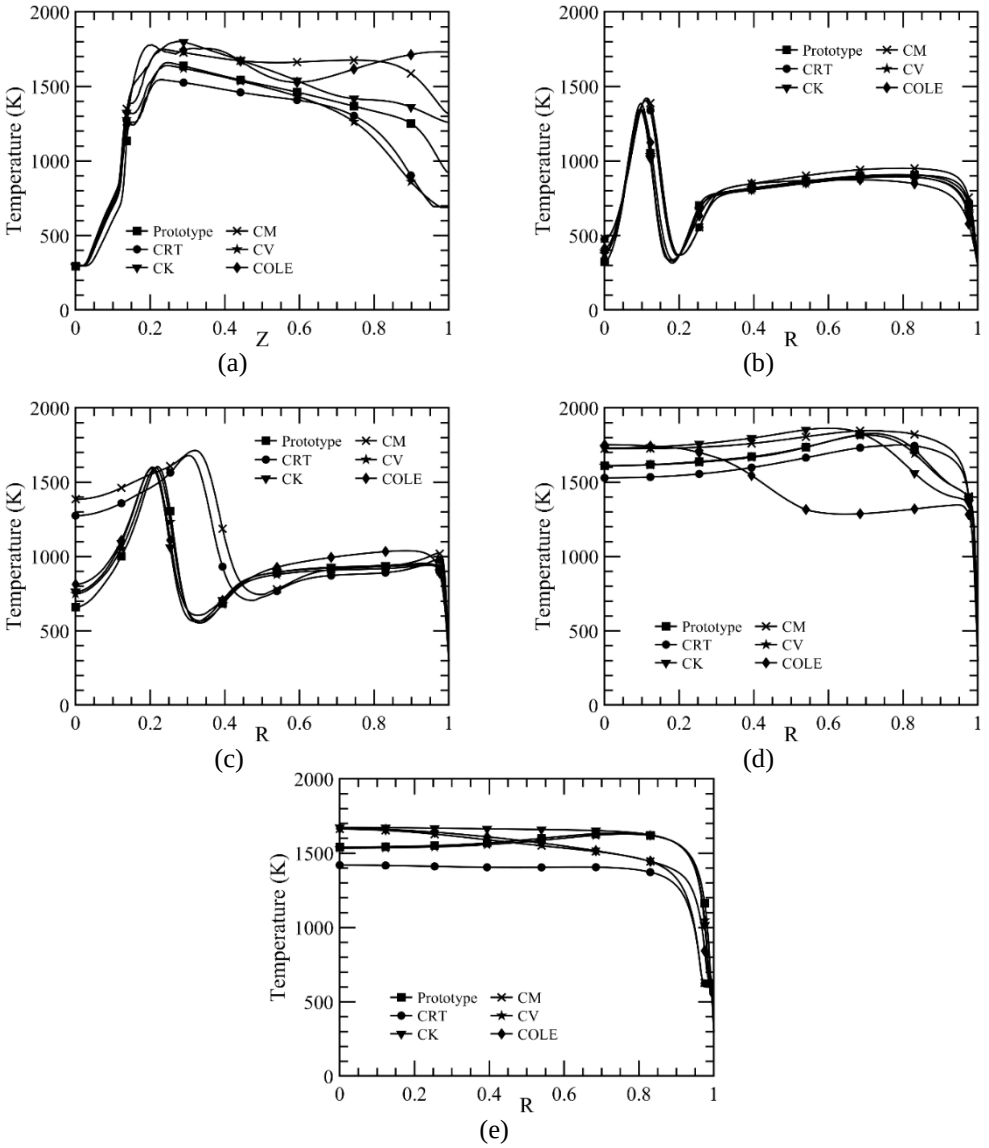

Figure 3. Scale-down studies, 50% energy input: (a) R = 0, (b) Z = 0.044, (c) Z = 0.11, (d) Z = 0.22 and (e) Z = 0.44

There is a clear distinction between two groups of profiles: the prototype, CV and CK versus CM and CRT. Examination of the temperature contour in Figure 4 reveals a downstream shift in the combustion core compared to the prototype. This shift results in higher temperature peaks for CRT and CK. The temperature differences diminish as the flow approaches the combustor wall. In Figures 3(d) and 3(e), the temperature profiles are much closer, with a maximum deviation of about 7% when comparing the prototype to CRT. This reduced difference can be attributed to the completion of the combustion process within the combustor. These deviations can be explained by the underlying flow physics, which depends on geometric dimensions and energy inputs. In the furnace studied, air and fuel expand radially upon entering the combustor, creating corner and central recirculation zones. These zones are clearly visible in stream traces and temperature contours shown in Figure 4. The strength, shape, and dimensions of these recirculation zones vary between scale-down models, leading to turbulence levels and effectiveness changes. As a result, reduced energy input and altered turbulence contribute to the temperature profile deviations observed in the scaled models compared to the prototype. Figures 3(b) through 3(e) compare radial temperature distributions at various nondimensional positions. Except for Z = 0.044, none of the scale-down approaches closely match the experimental temperature values. The primary causes of these deviations are altered flow characteristics and reduced energy input. Among all the scale-down models, the CRT model most accurately represents the overall trends of the temperature profile, particularly at nondimensional positions Z = 0.22 and Z = 0.44.

3.3 Comparison of Temperature Contours and Stream Traces

Figure 4 compares streamlines and temperature contours for specific cases with 50% of the total energy supplied for the scale-down with the prototypes. In each case of Figure 4(a) to 4(e), the upper part represents results obtained from the prototype, while the lower part indicates the contour distribution obtained from a specific case. As presented in Figure 4, all cases of scale-down methods produce three recirculation zones, except for the Cole method, where fluid velocities and energy input are lower. Of the three recirculation zones, two (corner recirculation zones) are in the corners, and one (central recirculation zone) is at the axis near the fuel and air jet entry. The central one is larger and more prominent among all recirculation zones, while the corner recirculation zone near the exit is weaker and smaller. This arrangement of vortices influences the main flow, causing it to bend towards the upper wall of the geometry. These vortices are critical in all scenarios, as they play a significant role in mixing fuel and air, flame holding, and fuel burning, which is essential for efficient combustion. The bending of the main flow towards the upper wall suggests that the flow dynamics are complex and that the design of the combustion chamber must accommodate these patterns to ensure optimal combustion.

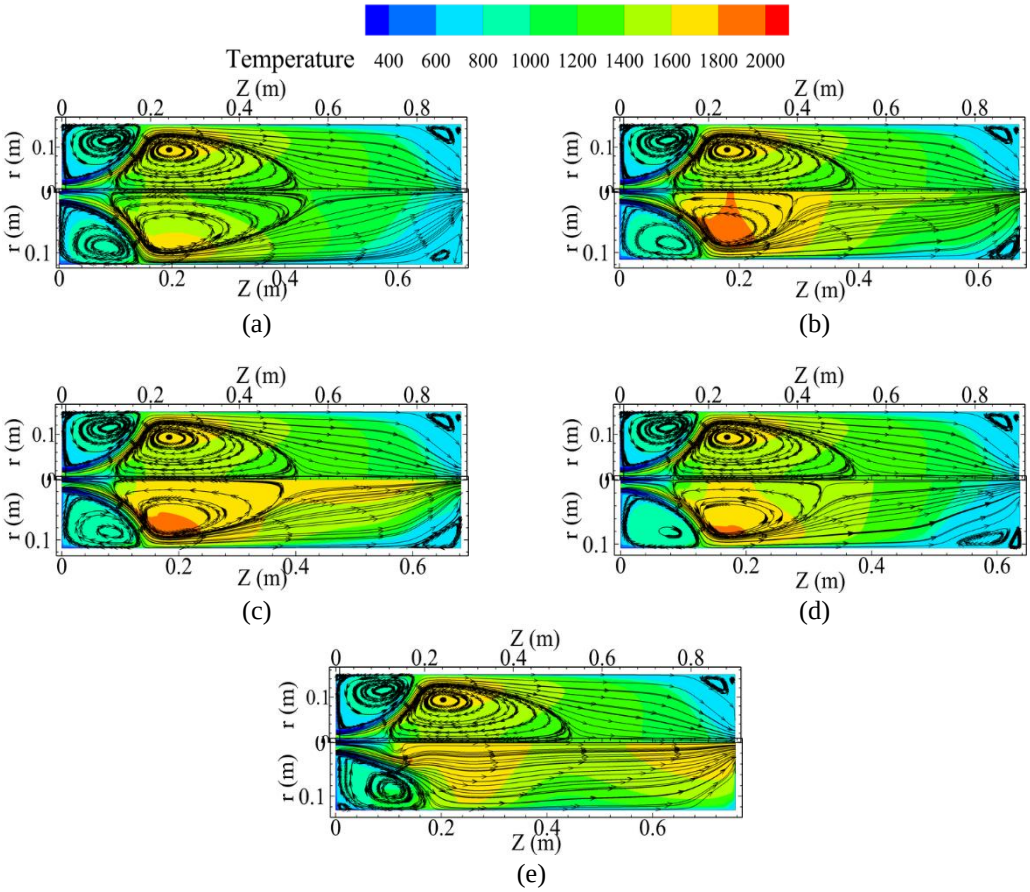

Figure 4. Stream trace and temperature distribution for 50% energy input with full-scale geometry: (a) CRT, (b) CK, (c) CM, (d) CV and (e) Cole

The expansion and acceleration of the flow at the outlet of the combustion chamber are also noteworthy, as these characteristics can impact the overall performance of the combustor, including its emissions and efficiency. The central

recirculation zones captured by the CK, CV and Cole methods are smaller than those in other scale-down geometries. Thus, the inappropriate prediction of this zone results in deviations in the temperature profile, as presented in Figure 3. Results for reduced energy input to 50% showed different combustor dimension values (R_{max}=126 mm to 106 mm, L = 756 mm to 636 mm), as tabulated in Table 1. The heat flux density, Q''' of 0.88 MW/m^3 for the full-scale geometry and the CRT method are the same but differ for other methods. The shape and size of the recirculation zone and temperature contours captured by the CRT method are comparable to those of the prototype. The CRT method also closely represents trends in temperature distribution, as shown in Figure 3. Thus, the CRT approach is the optimum choice for developing a scale-down model required for laboratory tests. The CRT method with 50% energy input results in a model geometry with an outer radius of 119.06 mm and a length of 714.33 mm. These dimensions are still large enough for a laboratory-scale model. To minimize the model dimensions further, the energy input is reduced to 7.30 kW. Table 3 represents the reduced model dimensions for this energy input. The outer radius reduces to 76.18 mm. Numerical simulations with these reduced dimensions are performed. Trends in the temperature profile are compared for the prototype, CRT with 50% energy input (D = 238.12 mm), CRT with a diameter of 152.4 mm (7.30 kW), and experimental results of Wilkes et al. [23].

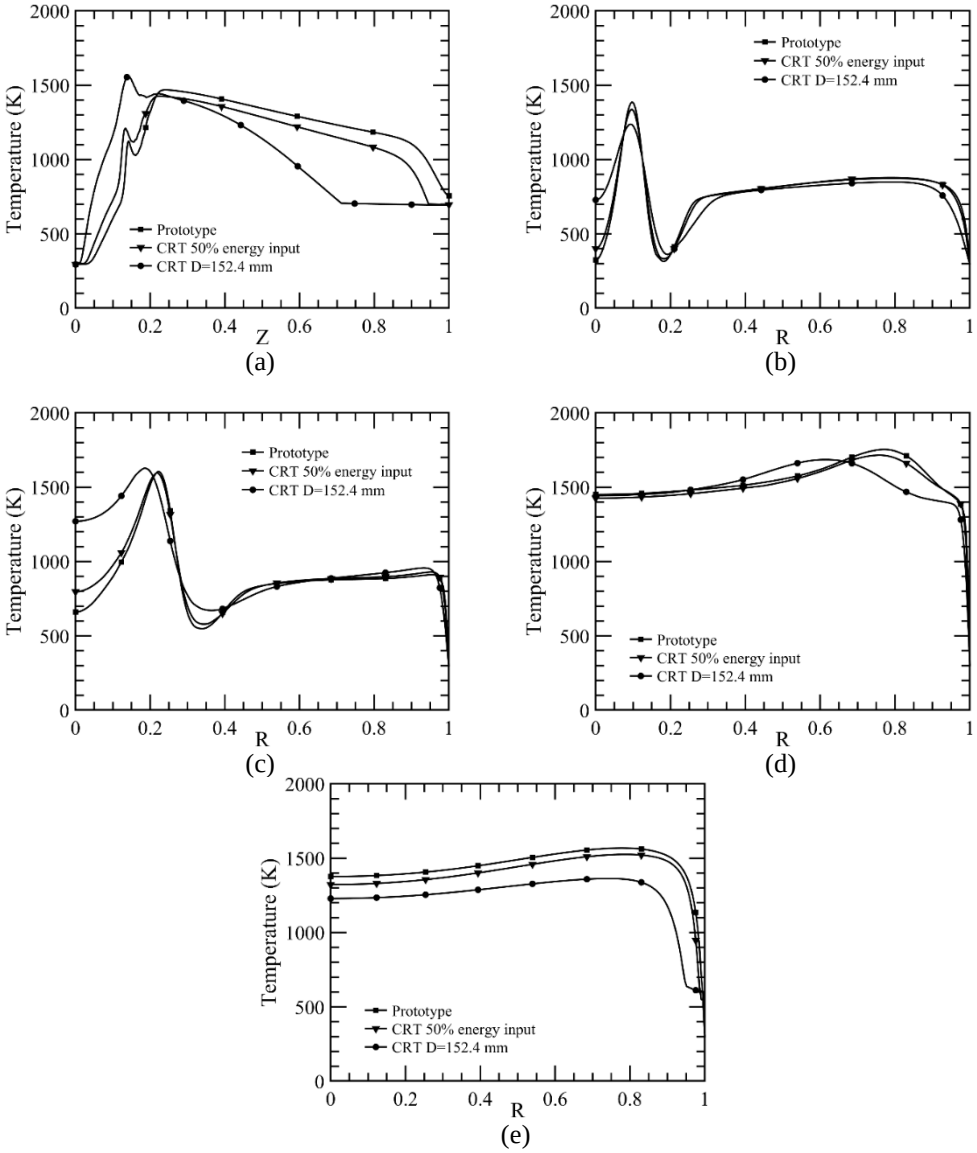

Figure 5. Axial and radial temperature distribution: (a) R = 0, (b) Z = 0.044, (c) Z = 0.11, (d) Z = 0.22 and (e) Z = 0.44

3.4 Comparison of Temperature Profile for CRT

A reactive numerical simulation is carried out for the model with dimensions and flow variable values shown in Table 3. A comparison of the temperature profiles is shown in figure 5. As shown in Figure 5(a), the predicted axial temperature profiles deviate considerably near the inlet and exit of the furnace geometry. For CRT (D = 152.4 mm), the deviation from the prototype results is maximum. In reactive physics, the increase in temperature also depends on the energy released and input. In CRT (D = 152.4 mm), the energy input is only 7.30 kW compared to 55.73 kW in the prototype. This low energy input is the primary reason for the lower maximum temperature value and significant deviation in CRT (D = 152.4 mm).

Table 3. Model dimensions and flow variable for D = 152.4 mm using the CRT method

Velocity Scaling Factor	---------	0.5079
Geometric Scaling Factor	---------	0.5079
	Full Scale	CRT
Q (kW)	55.73	7.30
U_f (m/s)	15.00	7.62
R_f (mm)	6.00	3.05
U_{air} axial (m/s)	12.80	6.50
U_t (m/s)	6.27	3.18
$R_{air\ inner}$ (mm)	16.50	8.38
$R_{air\ outer}$ (mm)	27.50	13.97
R_{outlet} (mm)	44.00	22.35
R_{max} (mm)	150.00	76.18
L (mm)	900.00	457.08
Q''' (MW/m^3)	0.88	0.88

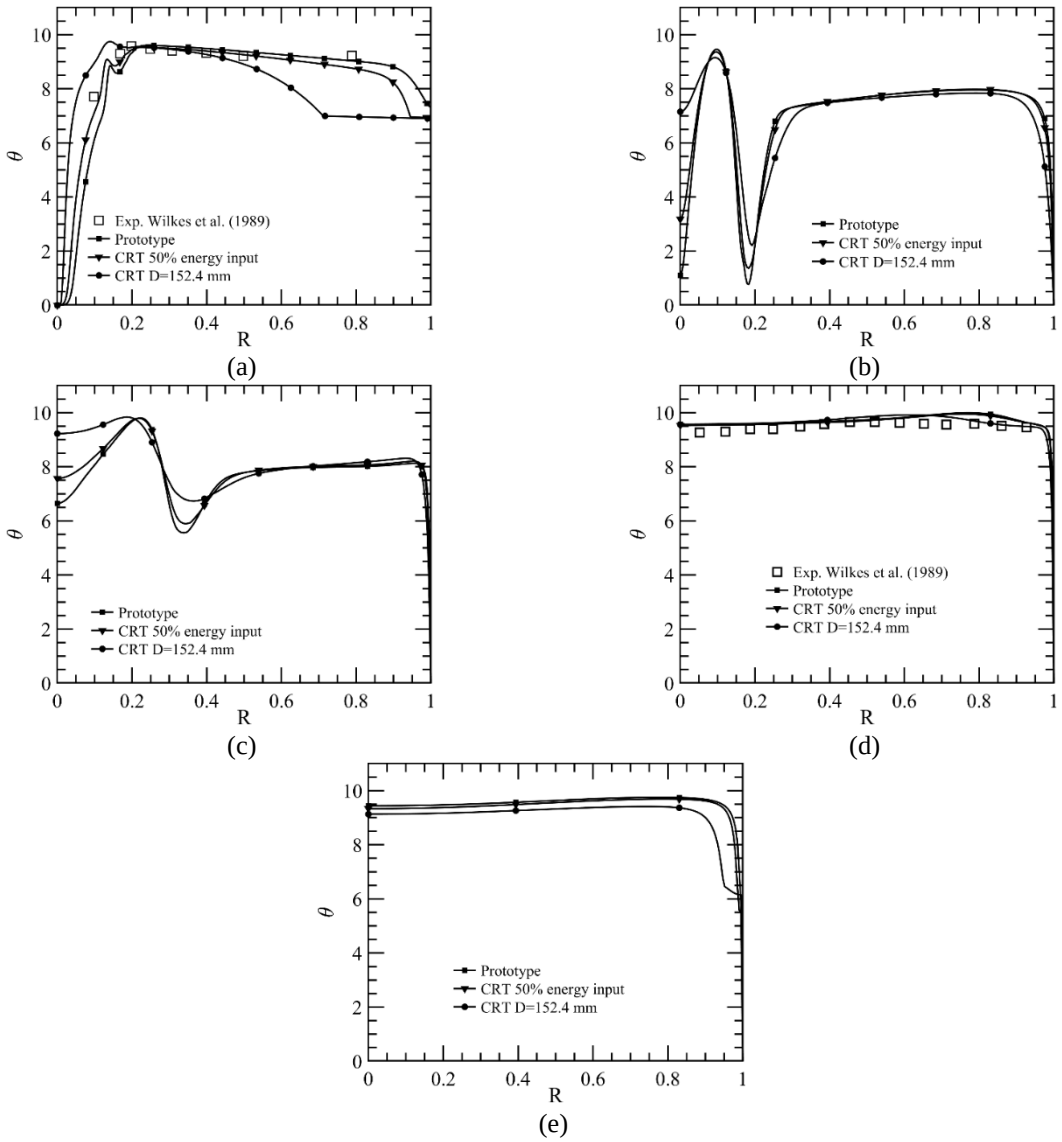

Figure 6. θ profiles for different non-dimensional locations: (a) R = 0, (b) Z = 0.044, (c) Z = 0.11, (d) Z = 0.22 and (e) Z = 0.44

Radial temperature profiles at station Z = 0.04 and Z = 0.11 are comparable with acceptable deviations. Significant deviation is observed at these stations up to the dimensionless position R = 0.2. At Z = 0.22, CRT (D = 152.4 mm) shows a noticeable difference compared to other cases. At the dimensionless position Z = 0.44, both scaled-down approaches

underpredict the temperature value; however, the trends in temperature distribution are comparable. Overall, there is a considerable deviation between the temperature profiles of CRT (D=152.4 mm) and that of the prototype. The temperature profile largely depends on the intensity of combustion, which is influenced by the rate of flow expansion from the inlet to the test section, the geometrical features of the combustor, the air-fuel ratio, the velocity of air and fuel at the inlet, the penetration of air and fuel into the test section, and other factors. Scale-down geometry suffers from reduced dimensions, low energy input, and weak heat generation. Due to this, the absolute temperature profiles of the prototype and scaled-down models do not match. A novel non-dimensional temperature profile is defined to address the above-mentioned dependency on temperature.

$$\theta = \frac{[(T_{cell} - T_{\infty})/(T_{adi} - T_{\infty})]}{[(T_{cell}\, C_P/CV)]} \tag{1}$$

where, T_{cell} is the respective cells' temperature obtained from numerical analysis, and Tadi is a particular fuel adiabatic temperature (2230 K). The C is the specific heat (2150.7 J/kg-K) of the air-methane mixture, CV is the calorific value of methane (50 MJ/kg), and T_{∞} is the inlet temperature (295 K). Variations of θ are plotted and presented for the experimental results of Wilkes et al. [24], scale-down methods CRT with 50% energy input and CRT (D = 152.4 mm).

3.5 Dimensionless Temperature Variations

A novel dimensionless variable, θ for temperature, addresses temperature dependency on energy generated and energy input to the reactive system. Variations θ are presented in Figure 6. Figure 6 (a) shows that θ variations are comparable for the experimental results, prototype, and CRT with 50% energy input. For CRT (D = 152.4 mm), there is a discrepancy in the θ profile between Z = 0.6 and Z = 0.8. The θ profile for Z = 0.011 for R is shown in Figure 6 (b) and indicates discrepancies in the vicinity of R = 0.2, while for other dimensionless radial positions, the trends of profiles match. A similar observation is made for temperature profiles at Z = 0.11 and Z = 0.44. Between R = 0.2 and R = 0.4, there are some deviations. θ profiles overlap for all the approaches at Z = 0.22. In Figures 6(a) and 6(d), the θ variation is compared with the experimental study of wilkes et al. [24] and the present simulation (prototype and CRT, 50% heat input, and D = 152.4 mm). The comparison reveals that the temperature profile agrees well with a maximum deviation of 17%.

4. CONCLUSIONS

In the present study, simulations are carried out for prototype and scaled-down geometries. Results are compared in terms of temperature profiles, temperature contours, and streamlines. A distinct dimensionless temperature variable, θ is defined, and trends in the axial and radial variations of θ are compared. The primary conclusions of the current study are as follows:

i) Scaled-down methods are suitable for reducing the prototype dimensions and generating laboratory-acceptable geometries. A comparison of flow and thermal variables at 50% energy input indicates that CRT outperforms other methods, such as CV, CM, CK, and Cole.

ii) At very low energy input, there is a large discrepancy between the temperature profile of CRT with 50% energy input and that of the prototype. Thus, the dimensional temperature predicted from the scaled model cannot effectively map the temperature variation for the prototype.

iii) A new dimensionless temperature, θ is defined based on energy input to the scaled geometry and energy generated by the respective cell. A comparison of axial and radial temperatures, θ reveals that the dimensionless approach helps map the scaled-down model temperature profile to the prototype. This approach works well with reasonable accuracy (with a maximum deviation of 17%), even at low energy input.

ACKNOWLEDGEMENTS

This study was not supported by any grants from funding bodies in the public, private, or not-for-profit sectors.

CONFLICT OF INTEREST

The authors declare no conflicts of interest.

AUTHORS CONTRIBUTION

A. B. Makwana (Methodology; Investigation; Writing & Validation)

Rupesh D. Shah (Review, Editing & Supervision)

AVAILABILITY OF DATA AND MATERIALS

The data supporting this study's findings are available on request from the corresponding author

ETHICS STATEMENTS

Not applicable

REFERENCES

[1] W. Xie, S. Ting, B. Ge, S. Zang, "Effects of scaling laws on flow and combustion characteristics of lean premixed swirl burners," *Journal of the Global Power and Propulsion Society*, vol. 6, pp. 343–353, 2022.

[2] E. Drubetskoi, S. Eckart, H. Krause, "Short overview on combustion systems scale-up with emphasis on NO_x emissions of gas-fired furnaces," *Energy Science & Engineering*, vol. 10, no. 2, pp. 621–629, 2022.

[3] J. A. Cole, T. P. Parr, N. C. Widmer, K. J. Wilson, K. C. Schadow, W. M. R. Seeker, "Scaling criteria for the development of an acoustically stabilized dump combustor," *Proceedings of the Combustion Institute*, vol. 28, no. 1, pp. 1297–1304, 2000.

[4] N. Suksam, J. Charoensuk, "Numerical investigation of the effect of constant velocity and constant residence time scaling criteria on the natural gas MILD combustion," *Journal of Thermal Science and Technology*, vol. 14, no. 2, pp. 1-16, 2019.

[5] C. Meraner, T. Li, M. Ditaranto, T. Løvås, "Effects of scaling laws on the combustion and NO_x characteristics of hydrogen burners," *Combustion and Flame*, vol. 214, pp. 407–418, 2020.

[6] V. Patel, R. Shah, "Effect of hydrogen enrichment on combustion characteristics of methane swirling and non-swirling inverse diffusion flame," *International Journal of Hydrogen Energy*, vol. 44, no. 52, pp. 28316–28329, 2019.

[7] M. Mohammadpour, M. Ashjaee, E. Houshfar, "Thermal performance and heat transfer characteristics analyses of oxy-biogas combustion in a swirl stabilized boiler under various oxidizing environments," *Energy*, vol. 261, p. 125206, 2022.

[8] S. Kasmaiee, S. Noori, S. Kasmaiee, "Numerical investigation of effective parameters in radiant heat transfer of oxyfuel combustion process of swirling gas furnaces," *Amirkabir Journal of Mechanical Engineering*, vol. 54, no. 7, pp. 1647–1672, 2022.

[9] D. C. Eaton, "Cruising economy by use of water injection," *Society of Automotive Engineers Transactions*, vol. 92, pp. 81–87, 1946.

[10] G. Tunç, İ. Yılmaz, "Comparison of the numerical models for the temperature distributions of non-premixed swirling methane flame," *Politeknik Dergisi*, vol. 22, no. 4, pp. 819–826, 2019.

[11] R. Weber, "Scaling characteristics of aerodynamics, heat transfer, and pollutant emissions in industrial flames," in *Symposium (International) on Combustion*, vol. 26, no. 2, pp. 3343–3354, 1996.

[12] S. Kumar, P. J. Paul, H. S. Mukunda, "Investigations of the scaling criteria for a mild combustion burner," *Proceedings of the Combustion Institute*, vol. 30, no. 2, pp. 2613–2621, 2005.

[13] R. K. Cheng, D. T. Yegian, M. M. Miyasato, G. S. Samuelsen, C. E. Benson, R. Pellizzari, et al., "Scaling and development of low-swirl burners for low-emission furnaces and boilers," in *Proceedings of the Combustion Institute*, vol. 28, no. 1, pp. 1305–1313, 2000.

[14] J. P. Smart, D. J. Morgan, P. A. Roberts, "The effect of scale on the performance of swirl stabilised pulverised coal burners," in *Symposium (International) on Combustion*, vol. 24, no. 1, pp. 1365–1372, 1992.

[15] G. Barroso, T. Nussbaumer, M. Ulrich, T. Reiterer, S. Feldmeier, "Scale-up methodology for automatic biomass furnaces," *Journal of the Energy Institute*, vol. 93, no. 2, pp. 591–604, 2020.

[16] T. C. Hsieh, A. Dahm, W. J. A, J. F. Driscoll, "Scaling laws for NO_x emission performance of burners and furnaces from 30 kW to 12 MW," *Combustion and Flame*, vol. 114, no. 1, pp. 54–80, 1998.

[17] R. Weber, M. Mancini, "On scaling and mathematical modelling of large-scale industrial flames," *Journal of the Energy Institute*, vol. 93, no. 1, pp. 43–51, 2020.

[18] S. Pramanik, R. V Ravikrishna, "Investigation of novel scaling criteria on a reverse-flow combustor," *Energy*, vol. 206, p. 118156, 2020.

[19] R. Weber, F. Breussin, "Scaling properties of swirling pulverized coal flames: From 180 kW to 50 MW thermal input," in *Symposium (International) on Combustion*, vol. 27, no. 2, pp. 2957–2964, 1998.

[20] M. Richter, J. Ströhle, and B. Epple, "Up-scaling of a laboratory-scale pulverised oxyfuel burner to semi-industrial-scale through a flow similarity approach," *Fuel*, vol. 371, p. 131809, 2024.

[21] W. Xie, T. Shi, B. Ge, S. Zang, "Experimental and numerical comparisons of geometric scaling criteria for lean premixed swirl combustor," *Physics of Fluids*, vol. 35, no. 9, p. 97119, 2023.

[22] W. Xie, T. Shi, B. Ge, S. Zang, "Numerical study on similarity performance of geometric scaling of lean premixed swirl combustor," *Physics of Fluids*, vol. 35, no. 9, p. 97121, 2023.

[23] N. S. Wilkes, P. W. Guilbert, C. M. Shepherd, S. Simcox, "The application of Harwell-Flow 3D to combustion models," *Atomic Energy Research Establishment Computer Science and Systems Division*, United Kingdom, Report Number AERE-R13508, 1989.

[24] M. Sadakata, Y. Hirose, "Scaling law for pollutant emission from a combustion furnace," *Fuel*, vol. 73, no. 8, pp. 1338–1342, 1994.

[25] B. E. Launder, D. B. Spalding, "The numerical computation of turbulent flows," *Computer Methods in Applied Mechanics and Engineering*, vol. 3, no. 2, pp. 269–289, 1974.

[26] A. A. Hosseini, M. Ghodrat, M. Moghiman, S. H. Pourhoseini, "Numerical study of inlet air swirl intensity effect of a methane-air diffusion flame on its combustion characteristics," *Case Studies in Thermal Engineering*, vol. 18, p. 100610, 2020.